11th International Workshop on Wave Hindcasting and Forecasting, Halifax, Nova Scotia, Canada, 2009.

# PRACTICAL NONLINEAR INTERACTION ALGORITHMS [1]

Hendrik L. Tolman[2]

NOAA / National Centers for Environmental Prediction
Environmental Modeling Center
Marine Modeling and Analysis Branch
Camp Springs, Maryland, USA

## 1 INTRODUCTION

For many years, the search has been on for practical nonlinear wave-wave interaction algorithms for operational wind wave models, where computational cost is a critical consideration. The particular challenge has been to replace the Discrete Interaction Approximation (DIA, Hasselmann et al., 1985, henceforth denoted as HHAB) with a more accurate approach without significantly increasing the computational costs of operational wind wave models. Since the publication of the DIA, computing capabilities have also increased dramatically, making more expensive parameterizations economically feasible. Even then, increased computational cost can only be justified when model behavior improves compared to model results obtained with the DIA. The present manuscript concentrates on effort from the National Centers for Environmental Prediction (NCEP). It represents a continuation of the work presented in Tolman and Krasnopolsky (2004), and is not intended to give a complete review of other work done in this field. NCEP has followed two different approaches to achieve more accurate yet economical approximations for the nonlinear interactions.

The first is the development of a Generalized Multiple DIA (GMD, Tolman, 2003, 2004, 2005, 2008) approach. The presentation will address how such a GMD can be formulated to properly scale over arbitrary depths up to relative depths $kd < 0.1$. In order to optimize such a GMD, a holistic approach is needed, where the entire wave model behavior is optimized. Previous holistic optimization methods for deep water have been expanded to include arbitrary water depths.

The second is the development of Neural Network Interaction Approximations (NNIA, Krasnopolsky et al., 2002; Tolman et al., 2005; Krasnopolsky et al., 2008). Previously, a hybrid NNIA has been presented with the capability to result in stable model integrations. This NNIA is presently expanded with a DIA-based filter technique to become faster and more stable. Effects of this filter and a more in-depth analysis of strengths and weaknesses of an NNIA will be discussed here.

The present report documents progress in both research efforts. Section 2 provides background information on wave models and interaction approaches. Sections 3 and 4 describe the Generalized Multiple DIA and its optimization. Section 5 describes recent progress in the Neural Network approaches, and Section 6 presents an outlook.

## 2 BACKGROUND

Wind wave model are generally based on a balance equation for spectral energy or action density (e.g., Hasselmann, 1960)

$$\frac{DF}{Dt} = S_{in} + S_{nl} + S_{ds} \quad , \tag{1}$$

where $F$ is an action or energy density spectrum of the wave field, retaining amplitude information only (assuming a random phase), and where $S_{in}$, $S_{nl}$ and $S_{ds}$ are source terms describing the three basic processes of wave growth due to wind, nonlinear wave-wave interaction, and wave energy dissipation due to wave breaking, respectively.

[1] MMAB contribution Nr. 280

[2] E-mail:Hendrik.Tolman@NOAA.gov

The spectral space of the action or energy spectrum in principle can be described with the wavenumber vector $\boldsymbol{k}$ with direction $\theta$ and norm $k$, and with the intrinsic (radian) frequency $\sigma$. Using an intrinsically linear description of the spectrum, a linear dispersion relation exists

$$\sigma^2 = gk \tanh kd \quad , \tag{2}$$

resulting in a two-dimensional spectral space. The spectral space can be described as, for instance, $(\boldsymbol{k})$, $(k, \theta)$ or $(\sigma, \theta)$. The former description is often used in theoretical work, the latter two in numerical models.

With the JONSWAP and SWAMP studies (Hasselmann et al., 1973; SWAMP group, 1985), the important role of the nonlinear interactions $S_{nl}$ in the wave growth process became apparent, as well as the need to accurately and explicitly describe this process in wind wave models. The interactions shift wave energy to lower frequencies (longer waves), and stabilize the high-frequency shape of the spectrum. Wave models with explicit parameterizations of $S_{nl}$ do not require assumption on the spectral shape (with the possible exception of a parametric tail at very high frequencies), and are generally identified as third-generation (3G) models. Previous (1G and 2G) models imply spectral shapes to model effects of nonlinear interactions.

The nonlinear interactions describe the conservative resonant exchange of action, energy and momentum between four spectral components (quadruplet) which satisfy the resonance conditions (Hasselmann, 1962, 1963) :

$$\boldsymbol{k}_1 + \boldsymbol{k}_2 = \boldsymbol{k}_3 + \boldsymbol{k}_4 \quad , \tag{3}$$

$$\sigma_1 + \sigma_2 = \sigma_3 + \sigma_4 \quad . \tag{4}$$

The interactions are conventionally expressed in terms of the rate of change of the action spectrum $n(\boldsymbol{k})$ as

$$\frac{\partial n_1}{\partial t} = \iiint G \, \delta_k \, \delta_\sigma \, P \, d\boldsymbol{k}_2 \, d\boldsymbol{k}_3 \, d\boldsymbol{k}_4 \quad , \tag{5}$$

where $n_i$ is the action density at component $i$, $n_i = n(\boldsymbol{k}_i)$, $G = G(\boldsymbol{k}_1, \boldsymbol{k}_2, \boldsymbol{k}_3, \boldsymbol{k}_4)$ is a complex coupling coefficient (Webb, 1978; Herterich and Hasselmann, 1980), $\delta_k$ and $\delta_\sigma$ are delta functions corresponding to the resonance conditions (3) and (4), and $P$ is the product term

$$P = n_1 n_2 \, (n_3 + n_4) - n_3 n_4 \, (n_1 + n_2) \quad . \tag{6}$$

A detailed balance exists between the changes of action energy and momentum at the four components of the quadruplet (Hasselmann, 1966; Komen et al., 1994, Section II.3.8). When considering discrete actions changes $\delta n_i$, this becomes particularly useful for numerical calculations as

$$-\delta n_1 = -\delta n_2 = \delta n_3 = \delta n_4 \tag{7}$$

introduces symmetry, enforces numerical conservation and reduces computations by a factor of four.

Equation (5) represents a six-dimensional Boltzmann integral. Application of the resonance conditions reduces this to a three-dimensional integral. Even in this form, the solution of the integral requires several orders of magnitude more computational effort than all other elements of a wave model combined. This implies that a 3G model based on Eq. (5) will be several orders of magnitude more expensive to run than a 1G or 2G model. Even if such a model would become economically feasible due to increasing computing capabilities, it would be hard to justify using such a model unless the corresponding 3G models is far superior to 1G and 2G models. Whereas 3G models appear to be more capable of reproducing combined wave fields (e.g., Hanson et al., 2009), they have yet to be shown to be far superior.

The introduction of the Discrete Interaction Approximation (HHAB) made the development of the first practical 3G models feasible (WAMDIG, 1988; Komen et al., 1994). Compared to the exact interactions, the DIA introduced the following simplifications:

1) A discrete version of the detailed balance form of the equations [cf. Eq.(7)] is used.

2) Integration of the multidimensional wavenumber space is replaced by computing discrete interactions for a representative quadruplet only. The representative quadruplet is define as

$$\left.\begin{array}{rcl} \boldsymbol{k}_1 & = & \boldsymbol{k}_2 \\ \sigma_3 & = & (1+\lambda)\sigma \\ \sigma_4 & = & (1-\lambda)\sigma \end{array}\right\} \quad , \tag{8}$$

where $\lambda$ is a constant, typically set to $\lambda = 0.25$. Contributions for the representative quadruplet are computed for $\boldsymbol{k}_1$ corresponding to each discrete point in spectral space.

3) Deep water is considered only. Effects of shallow water are partially accounted for by scaling the deep water interaction based on Hasselmann and Hasselmann (1981).

4) The complex coupling coefficient $G$ in Eq. (5) is replaced by a scaling function with a proportionality constant. With the deep water assumption, the scaling function as a function of $f$ and $g$ follows from simple dimensional considerations.

5) A logarithmic discrete frequency distribution is used in spectral space with

$$\sigma_{i+1} = X\sigma_i \quad , \tag{9}$$

This assumption allows for the removal (cancellation) of discrete bin sizes in the discrete DIA formulation, and hence is an integral part of the resulting DIA. Furthermore, together with the deep water assumption, it allows for discrete quadruplet layouts to be identical throughout the spectral grid, and hence fosters computational efficiency.

6) The DIA is derived explicitly for the energy or variance density $F(f,\theta)$ as a function of the frequency $f$ and direction $\theta$, with $F(f,\theta)/\sigma = n(f,\theta)$

Depending upon the other details of the wave model, the DIA typically is responsible for 40-75% of the computational effort required by the wave model. Various modifications to the original DIA have been suggested, including multiple representative quadruplets, alternative definitions of the representative quadruplet, and other spectral descriptions. For an overview of these, reference is made to Tolman (2008). The basic concepts and equations for the GMD are presented in Section 3, and the optimization of the GMD using a holistic approach is discussed in Section 4.

Another approach used to parameterize the nonlinear interactions is the use of Neural Networks. A precursor to this is the approach described in HHAB where an attempt is made to construct the interactions from Empirical Orthogonal Functions (EOFs). Tolman et al. (2005) used this decomposition approach combined with a Neural Network (NN) to successfully reproduce exact nonlinear interactions for test spectra (NN Interaction Approximation, NNIA). However, this approach does not result in stable model integration, since model spectra tend to diverge from training data sets used to develop the NNIA. Tolman and Krasnopolsky (2004) introduced a hybrid approach where an internal quality control in the NNIA identifies when the model integration diverges from the training data set, and then reverts to a full description of the interactions. This resulted in the first successful model integration with a NNIA. Recently, a nonlinear high-frequency smoothing algorithm was added to this compound NNIA, resulting in significantly better model results as illustrated in Section 5.

## 3 A GENERALIZED MULTIPLE DIA

A generalized multiple DIA (GMD) can be derived following the basic derivation of HHAB, but without implying deep water and without limiting the layout of the representative quadruplet. Such a generalized DIA was first addressed by Van Vledder (2002a), and was expanded upon by Tolman (2008). For details of the derivation of a Generalized Multiple DIA (GMD) reference is made to the latter report. Here, only major concepts and findings will be discussed. The two main goals are to generate more accurate parameterizations, and to obtain a DIA with appropriate behavior for arbitrary depths. Note that for deep water, a more generalized multiple DIA has already been shown to be significantly more accurate in representing interactions for selected spectra (Tolman, 2004; Tolman and Krasnopolsky, 2004).

The basis for any DIA is the discrete detailed balance version of Eq. (5), which can be written as

$$\begin{pmatrix} \delta n_1 \\ \delta n_2 \\ \delta n_3 \\ \delta n_4 \end{pmatrix} = \begin{pmatrix} -1 \\ -1 \\ 1 \\ 1 \end{pmatrix} B\, P\, \Delta\boldsymbol{k}\Delta t \quad , \tag{10}$$

where $P$ is the product term of Eq. (6), $B = B(f,\boldsymbol{k},g)$ is a scaling function including a proportionality constant, $\Delta t$ is a time increment, and $\Delta\boldsymbol{k}$ is a representative discrete phase space element. There are two main contributions to $B$. The first $B_1$ represent effects of going from a multi-dimensional integral to a single discrete representation, the second $B_2$ describes the scaling behavior of the coupling coefficient $G$.

Equation (10) represents discrete action changes $\delta n_i = \delta n(\boldsymbol{k}_i)$. They can be converted to source term contributions $\delta S_{nl,i} = \delta S_{nl}(\boldsymbol{k}_i)$ by dividing the discrete contribution by the time step and the discrete spectral bin size

$$\delta S_{nl,i} = \frac{\delta n_i}{\Delta\boldsymbol{k}_i \Delta t} \quad , \tag{11}$$

which, combined with Eq. (10) and after introducing

an explicit proportionality coefficient $C$, gives

$$\begin{pmatrix} \delta S_{nl,1} \\ \delta S_{nl,2} \\ \delta S_{nl,3} \\ \delta S_{nl,4} \end{pmatrix} = \begin{pmatrix} -\Delta\boldsymbol{k}/\Delta\boldsymbol{k}_1 \\ -\Delta\boldsymbol{k}/\Delta\boldsymbol{k}_2 \\ \Delta\boldsymbol{k}/\Delta\boldsymbol{k}_3 \\ \Delta\boldsymbol{k}/\Delta\boldsymbol{k}_4 \end{pmatrix} C\, B_1 B_2\, P \quad . \quad (12)$$

Note that HHAB assume that $\Delta\boldsymbol{k}$ and $\Delta\boldsymbol{k}_i$ are equivalent, thus allowing the discrete phase space elements to be canceled from the final equations. Note that $\Delta\boldsymbol{k}_i$ can vary in phase space, for instance according to Eq. (9), but that the latter equation then influences the final DIA and GMD expressions. Note, furthermore, that conversion to other spectral and phase space descriptions requires Jacobian transformations that generally results in modifications of $P$ and scaling terms than can be combined with $B = B_1 B_2$.

The following represent the major findings as discussed in detail in Tolman (2008), and in previous work as indicated.

1) The original quadruplet definition of HHAB is too restrictive to result in accurate interactions for selected spectra (Tolman, 2004). A symmetric quadruplet definition with maximum flexibility can be given as

$$\left.\begin{array}{rcl} \sigma_1 & = & (1+\mu)\sigma \\ \sigma_2 & = & (1-\mu)\sigma \\ \sigma_3 & = & (1+\lambda)\sigma \\ \sigma_4 & = & (1-\lambda)\sigma \\ \theta_2 & = & \theta_1 \pm \Delta\theta \end{array}\right\} \quad . \quad (13)$$

   For $\Delta\theta = \mu = 0$ this reverts to the original definition from the DIA, with $2\boldsymbol{k}_d = \boldsymbol{k}_1 + \boldsymbol{k}_2$, and $\boldsymbol{k}_d$ are discrete spectral phase space elements $\Delta\theta$ is implicitly defined and $\lambda$ and $\mu$ describe the quadruplet, otherwise all three parameters describe the quadruplet.

2) The expanded quadruplet definition does not result in stable model integration, unless used in a multiple DIA (Tolman, 2003, 2004)

3) Quadruplets with $\lambda$, $\mu$ and $\Delta\theta$ that result in valid quadruplets in deep water will result in valid quadruplets for arbitrary water depths if $0 \leq \mu \leq \lambda \leq 1$

4) If the quadruplet satisfies the resonance conditions for the actual depth, and if contributions to $S_{nl}$ are distributed to the discrete phase space analogous to bi-linear interpolation, energy, action and momentum are conserved. For continuous phase spaces, this was already observed by Webb (1978). In the quasi-deep water approach of the DIA, this implies that momentum is not conserved. Hence, to obtain a GMD with proper conservation properties, the quadruplet needs to be evaluated for each local relative depth at each discrete phase space element.

5) When converting to alternative spectral (phase space) description, the proper Jacobians in $P$ are essential to obtain reasonable behavior of the parameterization at arbitrary depth.

6) For deep water, a unique scaling behavior for $G$ can be found from its basic equations, identical to the scaling expression in terms of $f$ and $g$ as found on dimensional grounds. For restricted water depths this is not the case. Systematically different 'weak' and strong' interactions occur in deep and extremely shallow water. This can be modeled adequately in a GMD by defining the scaling function as the sum of asymptotic deep and shallow water expressions.

7) Similar arguments generally hold true for the residual scaling function $B_1$.

8) Changing spectral descriptions in principle has no impact on the computation of nonlinear contributions in a continuous phase space. However, when applied in a discrete phase space, the choice of spectral description influences whether properties of the quadruplet are evaluated at the phase space location of quadruplet elements or at discreet phase space locations. This proved to have a surprisingly large impact on the resulting interactions.

In Tolman (2008) a GMD is developed for the use in WAVEWATCH III $^{\mathrm{TM}}$. This model internally describes the wave field with the action density spectrum in terms of wavenumber and direction $N(k,\theta)$, with the spectral phase space defined with a logarithmic frequency distribution (9) invariant with depth (see Tolman and Booij, 1998). For this spectral description, the GMD contributions for a single representative quadruplet can be expressed as

$$\begin{pmatrix} \delta S_{nl,1} \\ \delta S_{nl,2} \\ \delta S_{nl,3} \\ \delta S_{nl,4} \end{pmatrix} = \begin{pmatrix} -1 \\ -1 \\ 1 \\ 1 \end{pmatrix} P \left( \frac{C_d B_d}{M_d} + \frac{C_s B_s}{M_s} \right) , \quad (14)$$

where $C_d$ and $C_s$ are the asymptotic deep and shallow proportionality constants. and where $M_d$ and

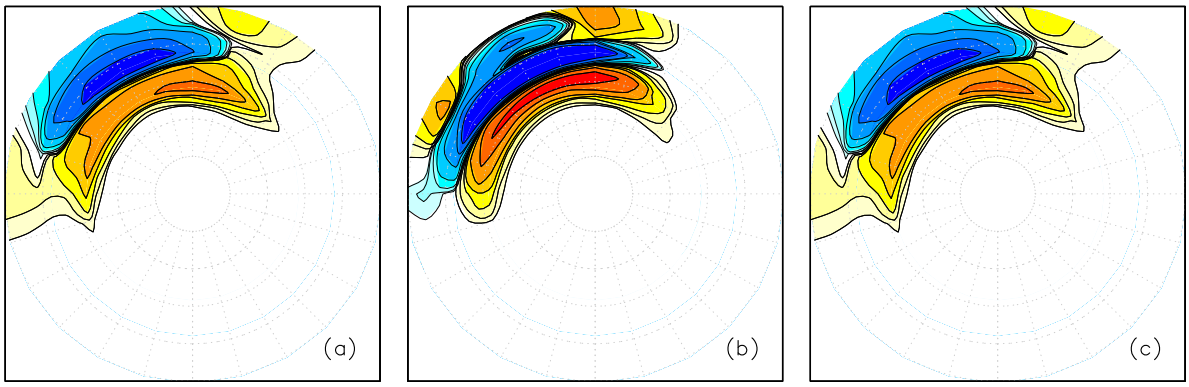


Fig. 1: Nonlinear interactions for a WAVEWATCH III $^{TM}$ test spectrum at 60m water depth from (a) DIA on which simulation was based, (b) exact interactions, and (c) GMD based on $F(f,\theta)$ [Eqs. (14), (18) - (20)]. Logarithmic scaling, red positive, blue negative, identical scaling for all panels.

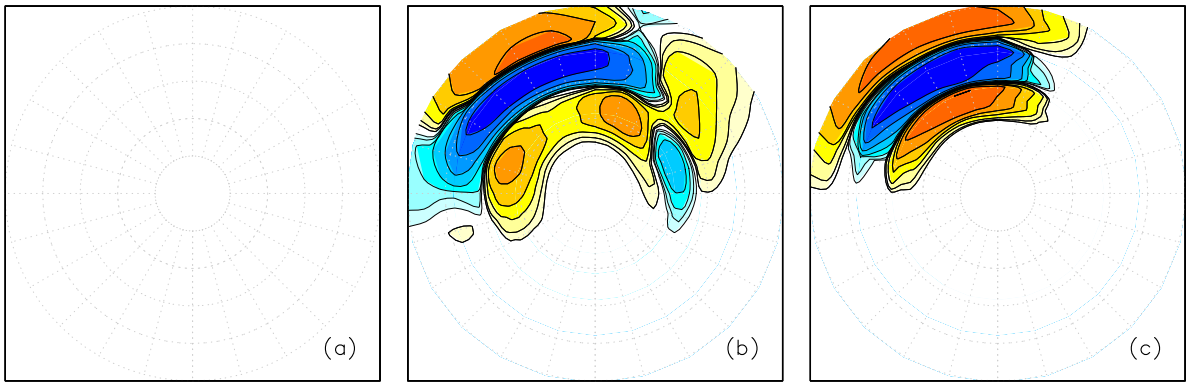


Fig. 2: Like Fig. 1 with water depth after model integration artificially reduced to 1m to simulate extremely shallow water. Lowest contour level increased by factor 1000 compared to Fig. 1.

$M_s$ are the corresponding number of active representative quadruplets. The latter scaling assures that a GMD with a set of identical representative quadruplets will be identical to a GMD with a single copy of that representative quadruplet. The product term $P$ in Eq. (14)is given as

$$\begin{aligned} P &= \frac{N_1}{k_1}\frac{N_2}{k_2}\left(\frac{N_3}{k_3}+\frac{N_4}{k_4}\right) \\ &- \frac{N_3}{k_3}\frac{N_4}{k_4}\left(\frac{N_1}{k_1}+\frac{N_2}{k_2}\right) , \end{aligned} \tag{15}$$

and asymptotic deep ($B_d$) and shallow water ($B_s$) scaling terms are given as (see Tolman, 2008)

$$B_d = \frac{k^{4+m}\,\sigma^{12-2m}}{(2\pi)^9\,g^{4-m}\,c_g} \quad , \tag{16}$$

$$B_s = \frac{g^2\,k^{10}}{(2\pi)^9\,c_g}(kd)^n \quad , \tag{17}$$

where $m$ and $n$ are tunable parameters in the scaling functions.

Alternatively, the GMD can be expressed in terms of the energy spectrum $F(f,\theta)$ consistent with the traditional DIA. For this spectral description, the corresponding source term is given by Eq. (14) and

$$\begin{aligned} P &= \frac{c_{g,1}F_1}{k_1\sigma_1}\frac{c_{g,2}F_2}{k_2\sigma_2}\left(\frac{c_{g,3}F_3}{k_3\sigma_3}+\frac{c_{g,4}F_4}{k_4\sigma_4}\right) \\ &- \frac{c_{g,3}F_3}{k_3\sigma_3}\frac{c_{g,4}F_4}{k_4\sigma_4}\left(\frac{c_{g,1}F_1}{k_1\sigma_1}+\frac{c_{g,2}F_2}{k_2\sigma_2}\right) , \end{aligned} \tag{18}$$

$$B_d = \frac{k^{4+m}\sigma^{13-2m}}{(2\pi)^{11}\, g^{4-m}\, c_g^2} \quad , \tag{19}$$

$$B_s = \frac{g^2\, k^{11}}{(2\pi)^{11}\, c_g}(kd)^n \quad . \tag{20}$$

The latter equations reproduce the original DIA (in deep water) if $F$ is interpolated from the discrete spectral space, but where $c_g(k\sigma)^{-1}$ are evaluated for the actual quadruplet components.

To illustrate the potential of the GMD a simple test case will be presented. Using the 'out-of-the-box' test case of WAVEWATCH III $^{\text{TM}}$ a model spectrum at 60 m water depth is generated. From this spectrum, the DIA interactions (used in the model integration), the exact interactions and the GMD interactions based on $F(f,\theta)$ with $\lambda = 0.25$ (single parameter quadruplet definition), $C_d = 10^7$, $C_s = 10^6$, $m = 4$ and $n = -3.5$ are computed. The latter parameter settings are tentative default settings from Tolman (2008), and should be nearly identical to the DIA in deep water. The results are presented in Fig. 1. As expected DIA and GMD results (Figs. 1a and c) are nearly identical, and are similar in shape and magnitude compared to the exact interactions (Fig. 1b).

To illustrate scaling behavior of the different approaches, shallow water conditions are artificially generated by considering the same spectrum and nonlinear parameterizations in a water depth of 1 m instead of 60 m. Resulting interactions are presented in Fig. 2 Exact interactions (Fig. 2b) in these extremely shallow conditions are three orders of magnitude larger than in the near-deep water conditions of Fig. 1. The interactions computed by the DIA (Fig. 2a) lag in strength by more than two orders of magnitude, making the source term invisible in panel (a). In contrast, the GMD (Fig. 2c) produces interactions with the proper magnitude and reasonable shape, even without detailed optimization. Hence, the GMD shows superior behavior compared to the DIA in extremely shallow water even if only a single representative quadruplet is used. Previously, Tolman and Krasnopolsky (2004) have shown that a multiple version of a DIA will significantly improve model behavior in deep water, when compared to a traditional DIA.

## 4 GMD OPTIMIZATION

Traditionally, parameterizations for nonlinear interactions have been tested and calibrated to accurately represent interactions for test spectra. However, this does not guarantee good behavior for model integration. For instance, the DIA does not represent interactions for test spectra very well, yet results in adequate model integration. Conversely, a DIA with expanded quadruplet definition with a single representative quadruplet works much better for individual test spectra, yet does not result in stable model integration (Tolman, 2004).

The above behavior can be attributed to the strongly nonlinear behavior of the interactions, combined with the inherent assumption of linear model behavior when working with test spectra only. To properly address the full nonlinear behavior of the interactions, parameterizations for the interactions need to be assessed in the context of full model integration, optimizing the full model results rather than the behavior for test spectra only. Such a 'holistic' optimization procedure was introduced by Tolman and Krasnopolsky (2004) and Tolman (2005). The present optimization approaches are an extension of the method introduced in the previous two papers. They will be described in full in Tolman (2009). The present manuscript will only outline the basic approaches and present some early results.

The holistic optimization has three key elements; (i) test cases to be considered, (ii) metrics to use in the optimization, and (iii) the actual optimization technique. In the previous papers the test cases consisted of deep water time- and fetch-limited growth. Metric considered were relative errors in the wave height $H_s$, and in the one- two-dimensional energy and steepness spectra, and the optimization was performed using genetic optimization techniques (e.g., Eiben and Smith, 2003). For the present study, all three basic approaches have been revisited.

Test cases considered are separate in deep and shallow water cases. The deep water cases, identified by number, include

- 01 Traditional time-limited growth.
- 02 Traditional fetch limited growth with wind perpendicular to the coast.
- 03 Time limited frontal page case of Tolman (1992).
- 04 Time limited case with constantly rotating wind.
- 05 Slanting fetch case with wind under 45° with coast.
- 06 Time-limited wave growth in the presence of swell.

The shallow water cases include

11 Time limited growth with stepwise reduced water depths.
12 Wind seas for onshore winds approaching a beach (1:250 beach slope, 1:1000 foreshore).
13 Swells approaching the same beach.

Metric for model assessment are based on prognostic parameters provided by the model. In the optimization procedure, mean parameters considered are the significant wave height ($H_s$), spectral peak frequency, mean direction and directional spread, high-frequency spectral energy level, frequency of no flux in nonlinear interactions, and the fit of the steepness spectrum in the high-frequency range of the spectrum. Added to this are one-dimensional spectral measure including the energy spectrum, steepness spectrum and (1-D) nonlinear interactions, and the mean direction and directional spread as a function of the spectral frequency. Finally, two-dimensional spectral parameters considered are the full energy and steepness spectrum and the full interactions. For each parameter an error measure is generated based on local normalization. For instance, for the wave height $H_s$ each data point for each test case is normalized as

$$\frac{H_{s,p} - H_{s,b}}{H_{s,b}} \quad , \tag{21}$$

where the indices $p$ and $b$ represent the results from the GMD parameterization and the baseline (exact) computations, respectively. By normalizing this way, relative errors in initial growth are considered equally important as relative errors for large sea states. When $N$ such data point are available per test case, the rms relative error per test case then typically is defined as

$$\epsilon_H = \sqrt{\frac{1}{N} \sum_N \left( \frac{H_{s,p} - H_{s,b}}{H_{s,b}} \right)^2} \quad . \tag{22}$$

Finally, a weighted sum of all error measures for each case produces a single error or score for each test cases, and scores for individual test cases can be combined into a single score or error measure in the same way. Initially mean wave parameter errors have been more heavily weighted to assure that critical measures like the significant wave height are well reproduced in the optimization procedure.

Optimizing the GMD involves many parameters to be optimized with many possible local minima of errors in the full parameter space. Due to local minima of errors, and possible discontinuous behavior of errors in parameter space, traditional steepest descent methods do not work well for this problem. An efficient way to attack this optimization problem is a genetic optimization approach as previously used in Tolman and Krasnopolsky (2004) and Tolman (2005). Genetic algorithms form a subset of what is generally identified as Evolutionary Computing (e.g., Eiben and Smith, 2003). In such methods, populations are described with the genome of individuals. Individuals in the population generate offspring using rules loosely based on natural reproduction, and the population retains only the most successful members, loosely following ideas of natural selection. This process has also been described as directed random search. Generally, approaches from the previous studies have been used here, with the exception that parameter space is described with real number rather than with bit strings. Note that a descent method can still be used seeded with good estimates from the genetic search routine. This allows for local convergence, and for a convergence test on the genetic approach.

It should be noted that independent of the optimization techniques used, optimization should be done in stages. First, deep water parameters can be optimized by considering deep water parameters only. For shallow water, optimum values for the deep water can then be kept constant while optimizing shallow water parameters.

Finally, a model and a baseline solution need to defined in and against which the GMD is optimized. The wave model will be the WAVEWATCH III ™ model with all its default settings (including shallow water source terms) except for the nonlinear interaction. As in previous parts of this study, the baseline results against which the GMD is optimized will be the Webb-Resio-Tracy (WRT) (Webb, 1978; Tracy and Resio, 1982; Resio and Perrie, 1991) method. Calculations are performed with the portable package developed by Van Vledder (2002b, 2006)[3]. Also needed is some reference DIA to establish the relative improvement obtained with an optimized GMD. Two reference DIAs will be considered. The first are the results obtained with the default DIA of the wave model ($\lambda = 0.25, C_d = 1.10^7$), henceforth referred to as the WW3 results. The second are results obtained with the traditional DIA settings from the WAM model (WAMDIG, 1988, $\lambda = 0.25, C_d = 3.10^7$), and will henceforth be denoted as WAM results.

[3] Model version 5.04 used here.

Table 1: Results of deep water optimization experiments for GMD. Error is mean error for cases 01, 03, 04, and 06.

| GMD base | quadruplet(s) $\lambda$ | $\mu$ | $C_d$ | error (%) |
|---|---|---|---|---|
| $N(k)$ | 0.226 | — | $1.39\,10^8$ | 48.6 |
| | 0.101 | 0.032 | $3.71\,10^8$ | |
| | 0.218 | 0.020 | $5.80\,10^7$ | 41.1 |
| | 0.441 | 0.232 | $4.63\,10^7$ | |
| $F(f)$ | 0.232 | — | $2.40\,10^7$ | 23.4 |
| | 0.070 | 0.025 | $8.13\,10^7$ | |
| | 0.108 | 0.080 | $3.99\,10^8$ | 17.6 |
| | 0.282 | 0.006 | $3.09\,10^7$ | |

In the present manuscript, only initial results of the holistic optimization will be presented. The main focus will be two-fold. First, a comparison will be made between the optimization potential of the GMD based on either $N(k)$ or $F(f)$. The former has the advantage of being closer to the original formulation of the nonlinear interactions, but the latter provides full backward compatibility with the DIA. Most importantly, however, is the final accuracy of the optimized approach. Second, a first indication of the optimization potential is given by focusing on two GMD configurations only; a minimal extension of the DIA with a single, single-parameter representative quadruplet, but fully optimized for all depths, and a two-parameter $(\lambda, \mu)$ three quadruplet configuration to asses optimization potential.

A first set of optimizations considers four deep water experiments; single parameter, single quadruplet layouts, and two-parameter $(\lambda, \mu)$ three quadruplet layouts for either the $N(k)$ or $F(f)$ based GMD. To facilitate quick turn around of these initial experiments, the fetch-limited deep water tests (02 and 05) have not been considered in the optimization experiments. For the single quadruplet layout, the population consists of 100 members, and only 10 generations are needed to come to convergence. For the three quadruplet layout, the population consists of 300 members, and 120 generations are considered. The best performing realization of the population is retained, and refined with a steepest descent method. The results of these optimization experiments are presented in Table 1.

From the results presented in Table 1 it is clear that the $F(f)$ representation of the GMD is far superior with respect to its capability to optimally represent the exact interactions in a full wave model. The failure of the $N(k)$ based GMD to do so is rooted in its inability to sustain the proper wave growth rates. This is illustrated in Fig. 3, which shows the wave heights for the latter GMDs (red lines) for test 01 to be severely underestimated compared to the baseline case (WRT, green), in spite of the model optimization. The previous DIA results (blue lines) do not show this deficiency. The corresponding spectra as presented in Fig. 4 indicate that spectral energy occurs at reasonable frequencies, but that spectral energy levels are not sustained by this GMD. The difference for the deep water test are sufficiently convincing to not consider further optimization of $N(k)$ based GMD, and instead consider the $F(f)$ based GMD only.

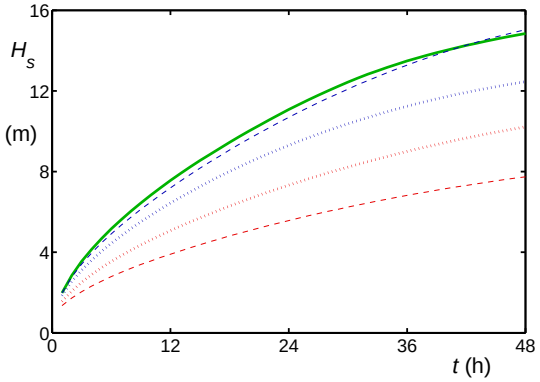


Fig. 3: Significant wave heights $H_s$ as a function of the time $t$ for test 01. for (a) the baseline case (WRT, green line), (b) the traditional DIA (blue lines; dashed: WW3, dotted: WAM) and the optimized GMD based on the $N(k)$ spectrum (red lines, dashed: one quadruplet, dotted: three quadruplets.

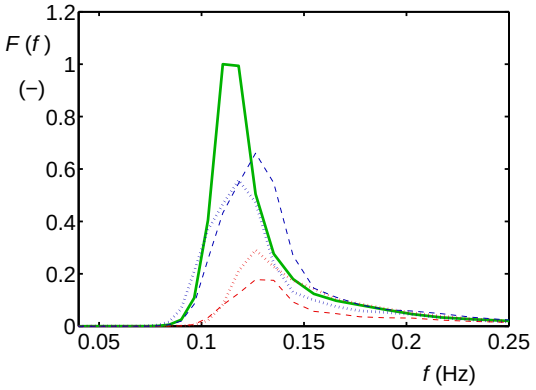


Fig. 4: One-dimensional spectra $F(f)$ for Fig. 3 after six hours of model integration.

Table 2: Results GMD configurations from shallow water optimization experiments for GMD, based on cases 11, 12, and 13. $F(f)$ based GMD using Eqs. (14) and (18) through (20).

| | GMD configuration | | | | | | error |
|---|---|---|---|---|---|---|---|
| | $\lambda$ | $\mu$ | $C_d$ | $C_s$ | m | n | (%) |
| WW3X | 0.250 | — | $1.00\,10^7$ | $3.53\,10^5$ | 0.16 | -3.50 | 43.4 |
| GMD1 | 0.232 | — | $2.40\,10^7$ | $3.10\,10^5$ | 0.40 | -3.50 | 41.6 |
| GMD3 | 0.070 | 0.025 | $8.13\,10^7$ | $7.91\,10^4$ | | | |
| | 0.108 | 0.080 | $3.99\,10^8$ | $2.34\,10^5$ | 0.02 | -3.50 | 44.1 |
| | 0.282 | 0.006 | $3.09\,10^7$ | $6.86\,10^5$ | | | |

Table 3: Overall errors in % for each test case for the traditional DIA (WW3, WAM), and for optimized GMDs (WW3X, GMD1, GMD3, see Table 2).

| | test case | | | | | | | | |
|---|---|---|---|---|---|---|---|---|---|
| | 01 | 02 | 03 | 04 | 05 | 06 | 11 | 12 | 13 |
| WAM | 26.2 | 25.1 | 23.1 | 24.2 | 25.4 | 34.7 | 23.9 | 29.0 | 83.2 |
| WW3 | 27.4 | 27.6 | 22.6 | 25.0 | 26.4 | 37.3 | 26.1 | 31.2 | 83.5 |
| WW3X | 27.4 | 27.6 | 22.5 | 25.1 | 26.5 | 37.3 | 24.6 | 31.0 | 74.5 |
| GMD1 | 22.3 | 21.9 | 18.9 | 20.2 | 20.6 | 32.2 | 21.0 | 29.5 | 74.4 |
| GMD3 | 13.7 | 15.3 | 13.7 | 13.2 | 17.0 | 30.0 | 14.4 | 21.6 | 96.2 |

With the initial optimization of the $F(f)$ based GMD for deep water, shallow water optimization will be considered. Three optimizations will be performed. First, the traditional deep water DIA as used in WAVEWATCH III $^{\text{TM}}$ will be expanded to shallow water, leaving the deep water setting unchanged. Hence, on quadruplet is considered with $\lambda = 0.25$ and $C_d = 1.\,10^7$, and $m$, and $C_s$ are optimized. This experiment is identified as WW3X. Second, this experiment is repeated with the optimum settings of $\lambda$ and $C_d$ from Table 1 (identified as GMD1). Note that $n$ could be optimized also, but is set to $n = -3.5$ to enforce scaling behavior in extremely shallow water. Finally, the two-parameter, three quadruplet deep water GMD defined in Table 1 is expanded to shallow water by optimizing $m$ and $n$ (single value for all quadruplets) and $C_s$ for each representative quadruplet (identified as GMD3). Note that the shallow water optimization considers tests 11, 12, and 13 only. A population with 100 members (150 for GMD3) and 10 (25) generations are considered, followed by a steepest descent method as described for the deep water test cases.

The resulting GMD configurations with their bulk errors are presented in Table 2, This Table indicates that the fully optimized GMD consistent with the DIA (GMD1) shows slightly better results than the GMD representing the traditional DIA in deep water but using optimized shallow water behavior of the GMD (WW3X).Somewhat surprisingly, the three-quadruplet GMD (GMD3) does not show better results. This will be discussed further below. Note that values of $C_s$ found in the optimization are consistent with Tolman (2008), but that values of $m$ are somewhat smaller ($m \approx 4$ expected). The latter may not be too surprising, since no strong dependency on $m$ is expected from the results of Tolman (2008).

Table 3 presents errors per test case for the various GMD configurations considered here. For individual test cases, additional optimization is generally shown to result in smaller errors. Several additional observations can be made from this Table.

First, the fetch-limited deep water test cases (cases 02 and 05) have not been used in the optimization, yet show systematic improvement with the test cases that have been actively optimized. This indicates the value of optimizing the wave model to idealized test cases, because cases not included in the optimization do improve in lockstep. For GMD3, however, these cases do not improve as much as the other cases, making the case for them to be included in the optimization.

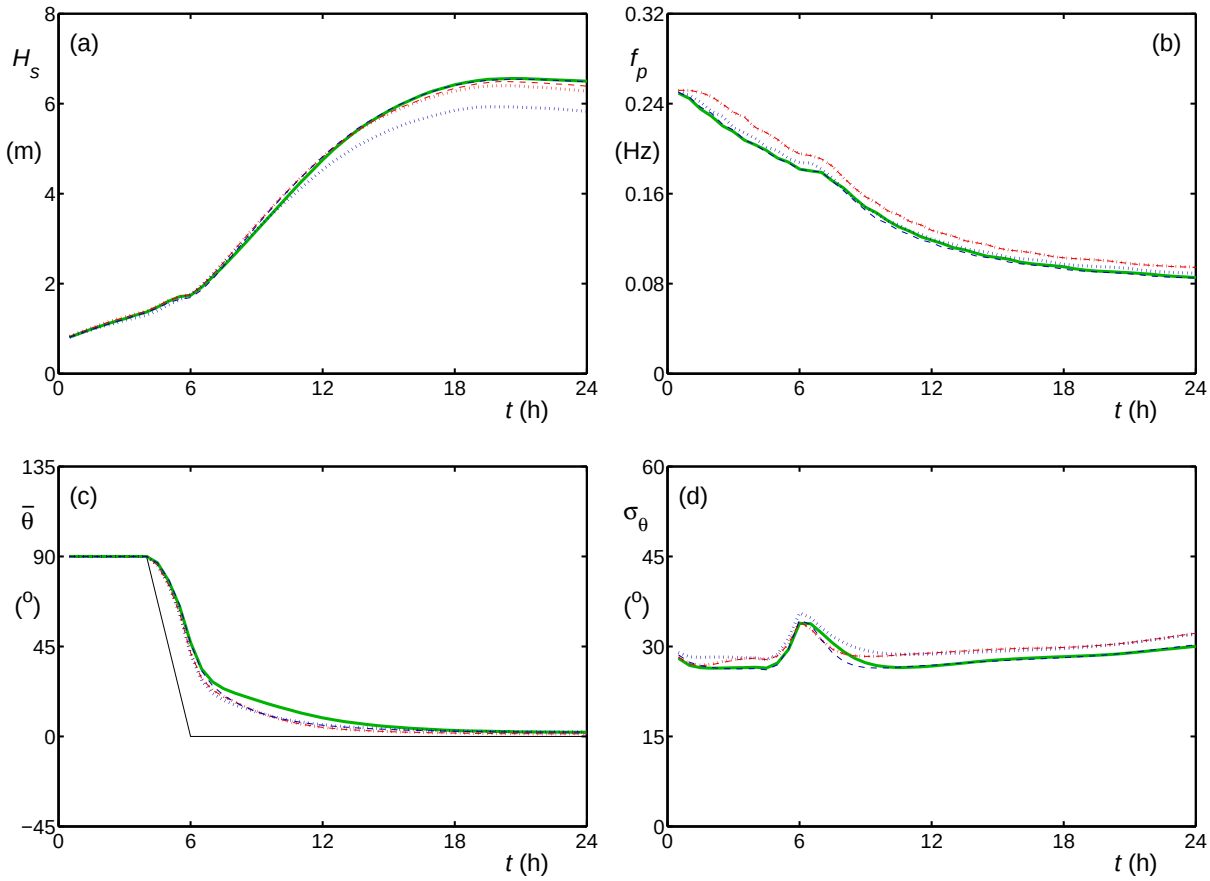


Fig. 5: Mean wave parameters for test 03. (a) Significant wave height $H_s$. (b) Peak frequency $f_p$. (c) Mean Direction $\overline{\theta}$. (d) Directional spread $\sigma$. Green line: WRT. Dashed red line: WW3. Dotted red line WW3X. Dotted blue line: GMD1. Dashed blue line: GMD3. Thin black line: wind direction.

---

Second, for deep water the WW3 and WW3X configurations consider identical equations for $s_{nl}$. However, the numerical implementations (DIA versus GMD) are vastly different. Together with the strongly nonlinear behavior of $s_{nl}$, this explains minor differences between resulting error of WW3 and WW3X for the deep water test cases 01 through 06. For shallow water, WW3X outperforms WW3 as expected.

Third, case 06 shows anomalously large errors compared to the deep water tests, in particularly the closely related test 01. This is die to erroneous differences in the swell conditions used in the baseline case (WRT) and in the GMD optimization. Because this has no impact on the general optimization beyond errors of the latter test case, this has not been corrected here.

Fourth, shallow water test case 13 shows anomalous behavior as it does not improve for the GMD3 configuration. This behavior is responsible for the increase overall shallow water error for GMD3 in Table 2. Note that the other two shallow water test (11 and 12) do show large improvement for GMD3. In this context, it is important to realize that the present study represents the first ever attempt at optimizing the shallow water aspects of the GMD, whereas much more experience is available for optimizing its deep water aspects (e.g., Tolman and Krasnopolsky, 2004; Tolman, 2005). Shallow water optimization will be addressed in much more detail in Tolman (2009).

As illustrations of the effects of the optimization, Figs. 5 and 6 show mean wave parameters for the WRT, WW3, WW3X, GMD1 and GMD3 ap-

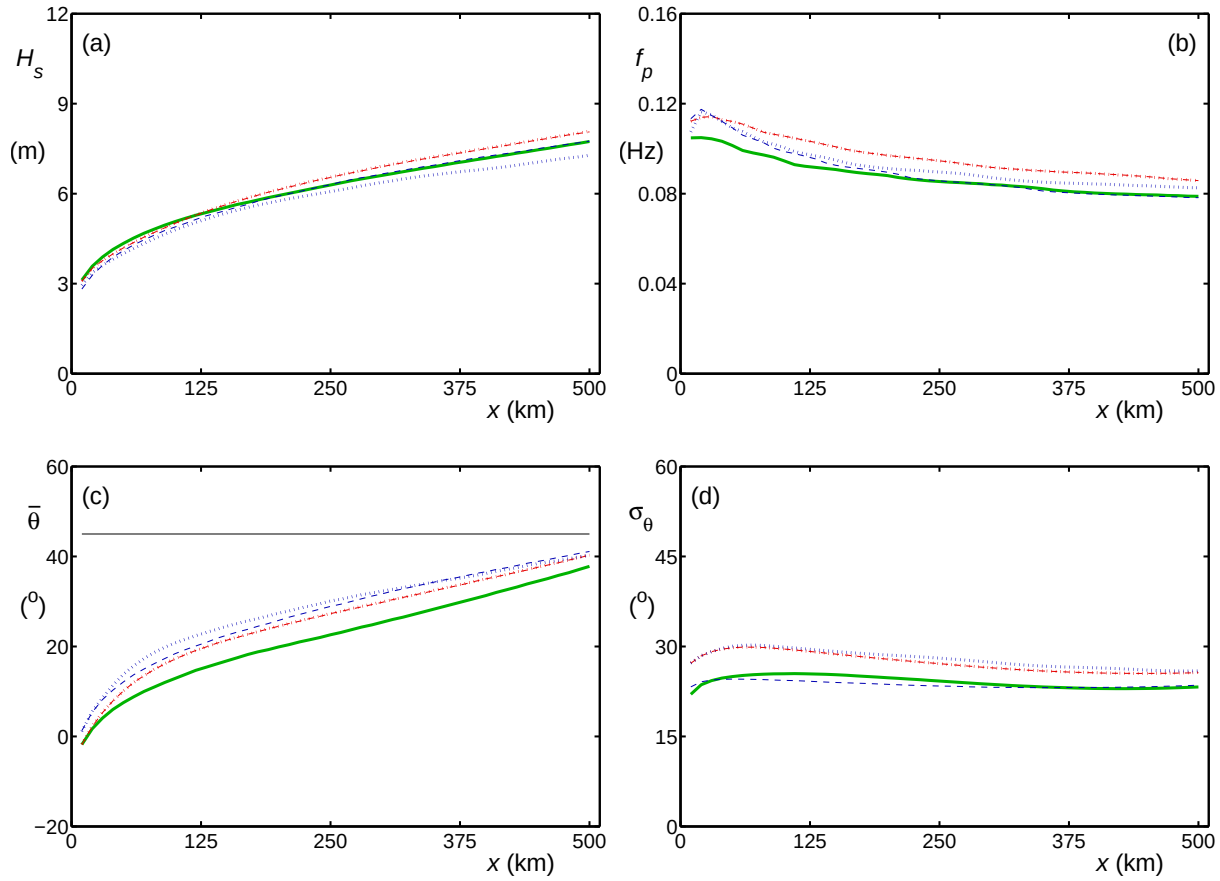


Fig. 6 : Like Fig. 5 for test 05.

proaches, for a test that was included in the optimization (test file 03), and for a test that was not included (test 05).

For test 03 the traditional DIA and the equivalent GMD (WW3 and WW3X, red lines), show an excellent reproduction of the exact (WRT, green lines) wave heights $H_s$, and moderate but notable deficiencies in the peak frequency $f_p$, mead direction $\overline{\theta}$ and directional spread $\sigma_\theta$. The equivalent fully optimized GMD (GMD1, dotted blue lines) shows improved behavior of the peak frequency $f_p$, and directional spread $\sigma_\theta$, at the cost of a poorer description of the wave height $H_s$. GMD3 shows no improvement of the mean direction compared to WW3X or GMD1.

Test 05 (Fig. 6) represents a case that has not been used in the present optimization experiments. As with test 03, the most complex optimized GMD (GMD3) shows better results than the more traditional GMDs and DIAs (WW3, WW3X, and GMD1). The exception is the mean direction, where all four approximations show similar errors when compared to the exact WRT solutions. The comparable behavior for this test indicates that optimizing a GMD to idealized cases should translate in better behavior for other cases, but the lack of improvement for the mean direction for GMD3 suggests that more can be gained if this test is used in the optimization. These results are consistent with the discussion of Table 3 above.

Figure 7 shows various one-dimensional spectral measures for test 03 after 6 h of model integration (compare to Fig. 5). The most complex GMD (GMD3, blue dashed line) shows significant improvements over simpler DIA and GMD approaches, particularly for the spectra $F(f)$ and $G(f)$, the directional spread and the nonlinear interactions. For the latter parameter, only the GMD3 reproduces the dual positive peak at low frequencies as displayed by the exact solution (WRT, green line).

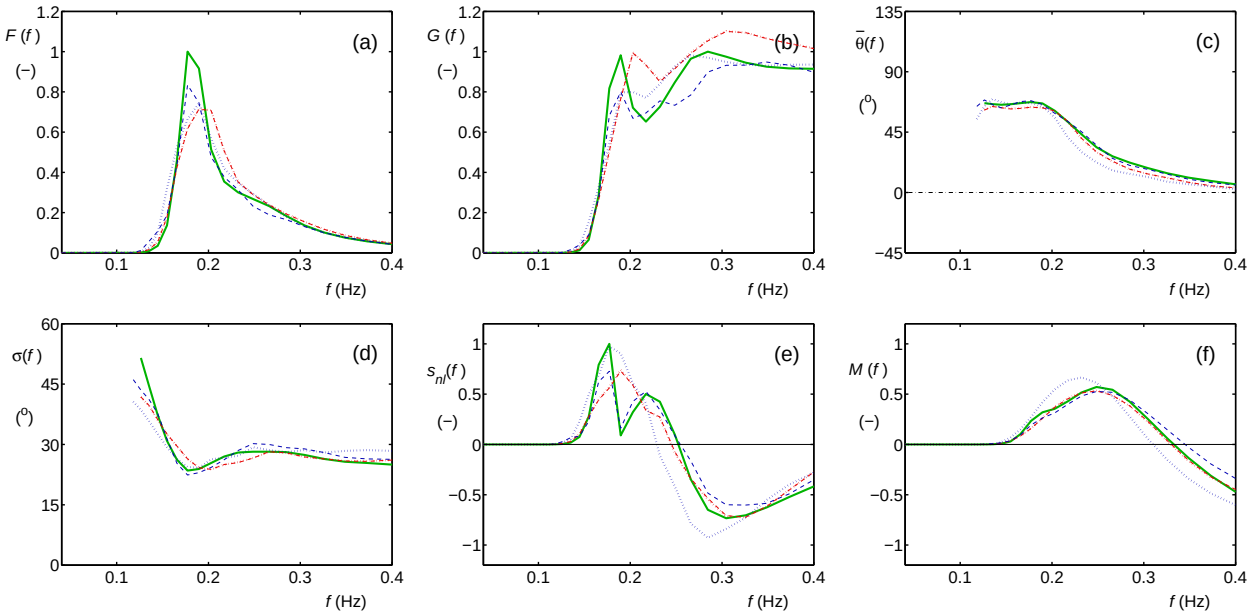


Fig. 7: One-dimensional spectral wave parameters for test 03 after 6 h of model integration.. (a) Spectrum $F(f)$. Steepness spectrum $G(f) = k^2F(f)$. (c) Mean direction $\theta(f)$. (d) Directional spread $\sigma(f)$. (e) Directionally integrated interactions $s_{nl}(f)$. (f) Nonlinear energy flux in frequency space $M(f)$. Legend as in Fig. 5. Chain line in panel (c) represents wind direction. Panels normalized with maximum value for WRT.

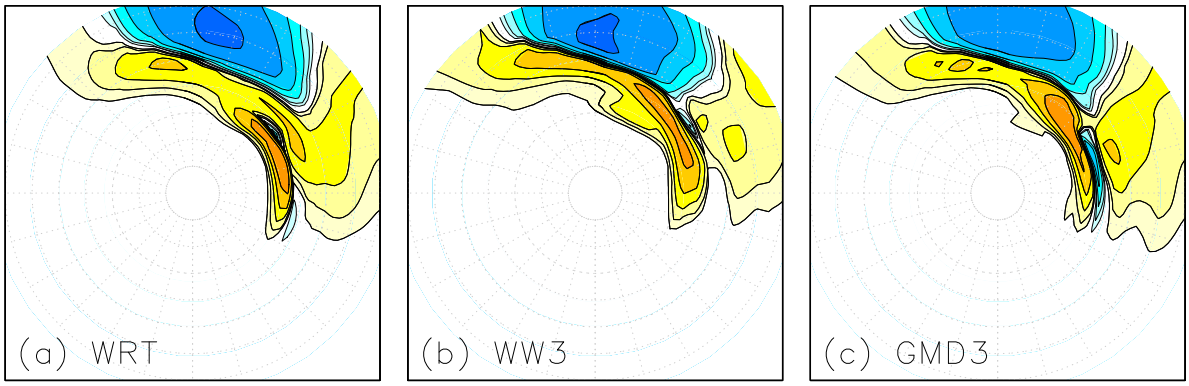


Fig. 8: Nonlinear interactions corresponding to Fig. 7e for (a) WRT, (b) WW3, and (c) GMD3 approaches. Logarithmic scaling, red positive, blue negative, identical scaling for all panels.

Figure 8 shows the full two dimensional nonlinear interactions corresponding to Fig. 7e for the exact (WRT), DIA (WW3) and GMD (GMD3) methods. Upon casual inspection, the three interactions look very similar. Close inspection, however, shows that the GMD3 interactions retain much more detail from the WRT interactions than the WW3 interactions, explaining the large difference found in Fig. 7e.

Finally, Fig. 9 presents spectra for test 13, representing swell on a beach in extremely shallow water. Note that the WW3 method (red dashed line) effectively ignores the corresponding strong interactions. Thus differences between the WRT (green lines) and WW3 methods identify the nett effect of the nonlinear interactions. At 6 m water depth (Fig. 9a), the interactions start influencing the spectral shape. At 3 m the spectral shape is strongly influenced. All DIA based approximations used here result in a disintegration of the spectrum, tentatively suggesting that more quadruplets are needed to describe the interactions (based on the experience gained with Tolman, 2005).

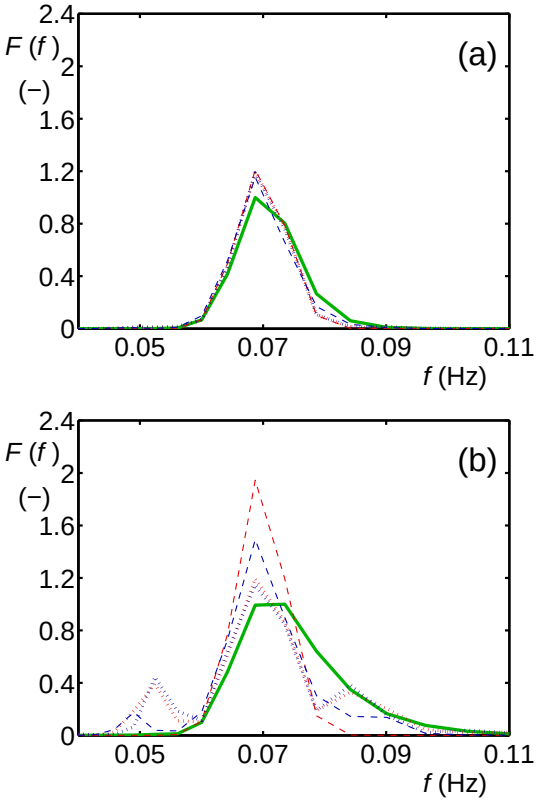


Fig. 9: One-dimensional spectra $F(f)$ for test 06 at (a) 6 m water depth and (b) 3 m water depth. Legend as in Fig. 5.

Conventionally, the four-wave (quadruplet) interactions are assumed to be small compared to three-wave (triad) interactions in extremely shallow water. The present results suggest, however, that four-wave interactions can have a significant impact on the spectral shape in severely depth-limited conditions.

It should again be noted that the optimization experiment presented here only represent the tip of the iceberg with respect to systematic optimization of the GMD, in particular with respect to the strategies used to optimize all free parameters. A more in-depth approach will be presented in Tolman (2009).

## 5 NEURAL NETWORKS

In a Neural Network Interaction Approximation (NNIA), a direct mapping of the interactions on the spectrum is pursued. A precursor to recent mapping approaches can be found in HHAB, where an interaction approximation based on Empirical Orthogonal Functions (EOF) was suggested. Efforts at NCEP to develop an NNIA are documented in (Krasnopolsky et al., 2002, 2003; Tolman and Krasnopolsky, 2004; Tolman et al., 2005; Krasnopolsky et al., 2008). Similar studies working to a NNIA have also been reported in Wahle et al. (2009).

The basic design of the present NNIA is described in Tolman and Krasnopolsky (2004) and is illustrated here in Fig. 10, which is reproduced from the latter paper.

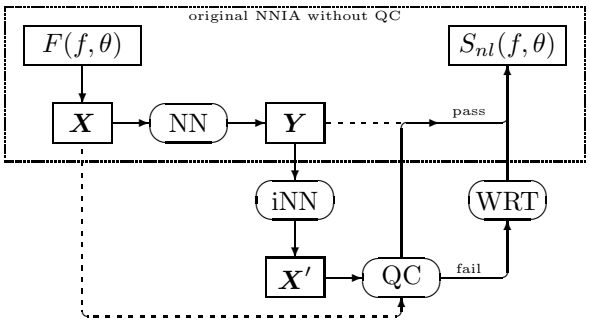


Fig. 10: Layout of a hybrid or compound NNIA, reverting to the WRT algorithm in cases where the quality control (QC) indicates failure of the NN. $\boldsymbol{X}$ and $\boldsymbol{Y}$ contain decomposition coefficients for the normalized spectrum $\tilde{F}$ and source $\tilde{S}_{nl}$. From Tolman and Krasnopolsky (2004).

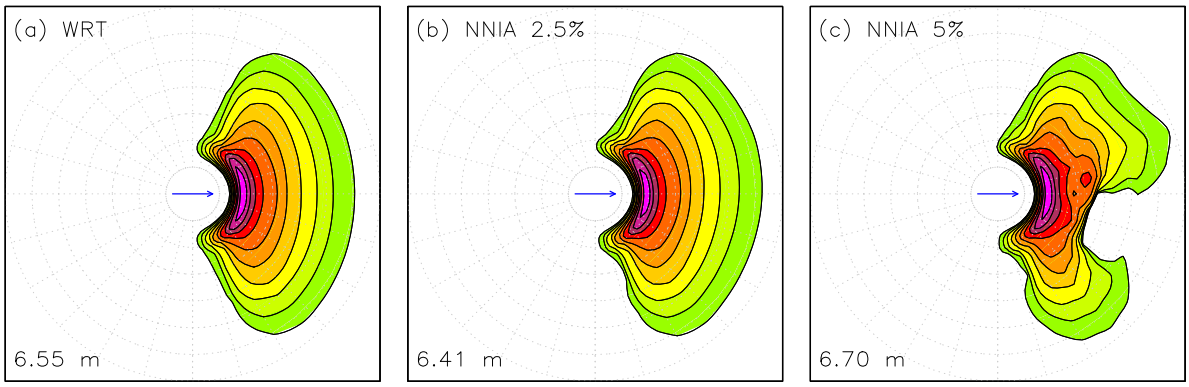


Fig. 11: Spectra for a homogeneous growth case with constant wind with $U_{10} = 20\,\mathrm{ms}^{-1}$ After 12h of model integration. (a) Exact (WRT) solution. (b) NNIA with maximum error in QC $\epsilon_{\max} = 2.5\%$. (c) NNIA with $\epsilon_{\max} = 5\%$. Identical logarithmic scaling in all panels. Wave heights $H_s$ depicted in lower left corner of each panel. No high frequency filtering.

In an NNIA, a Neural Network (NN) is used to describe the mapping between the spectrum and the source term. Although this mapping can be done considering the spectrum and source term directly (e.g., Wahle et al., 2009), proper scaling can be enforced independent of the mapping by applying the NN to normalized spectra and source terms Normalizing with an energy density ($F_n$), frequency ($f_n$) and direction ($\theta_n$), results in the following normalized parameters identified as $\tilde{F}$, etc.

$$\tilde{F}(\tilde{f},\tilde{\theta}) = F_n^{-1}\, F(f,\theta) \quad , \tag{23}$$

$$\tilde{S}_{nl}(\tilde{f},\tilde{\theta}) = g^4\, F_n^{-3}\, f_n^{-11}\, S_{nl}(f,\theta) \quad . \tag{24}$$

$$\tilde{f} = f_n^{-1}\, f \quad , \tag{25}$$

$$\tilde{\theta} = \theta - \theta_n \quad . \tag{26}$$

Initial development of the NNIA focuses on its most critical capabilities, i.e., the reproduction of wave growth. Hence, theses studies concentrate on single peaked wind sea spectra for which $F_n$, $f_n$, $\theta_n$ are naturally defined as their spectral peak values.

To reduce the dimensionality of the NN, it is applied to coefficients $\boldsymbol{X}$ and $\boldsymbol{Y}$ from a decomposition of the spectrum and source term

$$\tilde{F} \rightarrow \boldsymbol{X} \quad , \quad \tilde{S}_{nl} \rightarrow \boldsymbol{Y} \quad . \tag{27}$$

In Tolman et al. (2005) Empirical Orthogonal Functions (EOFs, Lorenz, 1956; Jolliffe, 1986) were established as efficient basis functions for the NNIA. With the adoption of EOFs, this NNIA can be considered as a generalization of the EOF based approach discussed in HHAB.

The development of an NN consists of a process called training. In this process, the NN is optimized using a large set of spectra and the corresponding exact (WRT) interactions. In the most recent attempts to develop an NNIA, training is performed using spectra and source terms from a one-point WAVEWATCH III $^{\mathrm{TM}}$ model representing time limited wave growth for constant or slowly varying wind speed and direction. In the latter case conditions are varying sufficiently slow to assure that the spectrum remains unimodal. The cost of the resulting NNIA proved comparable to that of the DIA, with nearly all the computational effort spend in the decomposition of $\tilde{F}$ into $\boldsymbol{X}$ and the construction of the source term $\tilde{S}_{nl}$ from $\boldsymbol{Y}$.

By nature, it is impossible to train the NN for all possible spectra, even if only wind seas are considered. It is, therefore, not expected that the the NNIA will always give appropriate results. Fortunately, it has been proven possible to estimate when the NN is not accurate, by estimating $\boldsymbol{X}$ (denoted as $\boldsymbol{X}'$) from $\boldsymbol{Y}$ using an 'inverse' NN (iNN). If $\boldsymbol{X}$ and $\boldsymbol{X}'$ diverge too much, the NN is inaccurate, and the source term should be estimated from the original (in this case WRT) algorithm. Such an hybrid or compound algorithm (e.g., Krasnopolsky et al., 2008) proved to be the first NNIA application able to produce stable albeit noisy wave growth in a numerical model in Tolman and Krasnopolsky (2004).

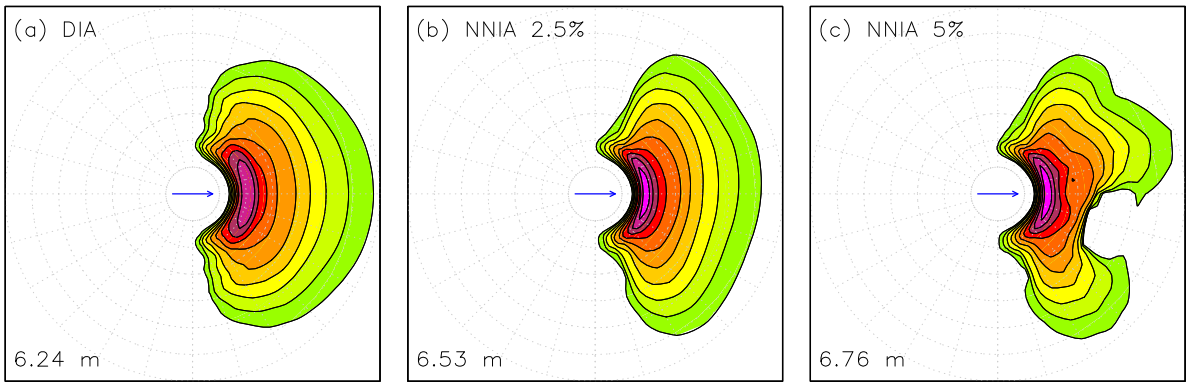


Fig. 12: Like Fig. 11 with high-frequency filtering added for NNIA. (a) represents classical DIA without filtering.

An additional benefit of introducing the explicit quality control (QC) to the NNIA is that spectra for which the NNIA does not work properly are identified automatically. This provides a natural method to incrementally increase the training data sets for the NNIA, targeting new spectra not sufficiently represented in the previous training data sets.

Figure 11 shows spectra from a homogeneous wave growth test with constants wind speeds $U_{10} = 20\,\mathrm{ms}^{-1}$. These results are comparable to Fig. 7 of Tolman and Krasnopolsky (2004), with the exception that the latter case was included in the NN training, whereas the present test is not. For a maximum allowed error in the QC of $\epsilon_{\max} = 2.5\%$, the spectrum and wave height produced with the NNIA are nearly identical to those obtained with the exact (WRT) method (compare Figs. 11a and b). For maximum allowed errors of $\epsilon_{\max} = 5\%$ (Fig. 11c), stable wave growth is found, but with clear deficiencies to the spectral shape. These results are consistent with those presented in Tolman and Krasnopolsky (2004).

The deficiencies in (Fig. 11c) are tentatively attributed to the inability of the NNIA to simultaneously describe large-scale features of the interactions resulting in spectral evolution, and small scale features stabilizing the shape of the spectral tail. The latter are essentially treated as noise by the NNIA, and rather than such features stabilizing the spectral shape, they result in accumulation of 'noise' (see also HHAB). In (Fig. 11c) this results in a 'hole' in the spectrum at higher frequencies. For (Fig. 11b) it results in minor oscillation in the high-frequency part of the spectrum (figures not presented here).

A simple way to address this hypothesis, is to add an explicit noise filter for high frequencies to the model integration. Tentatively, such a filter should be consistent with the interactions, and could be based on previously suggested diffusion approximations to the nonlinear interactions (e.g., HHAB, Zakharov and Pushkarev, 1999; Jenkins and Phillips, 2001). A more simple approach, using an unresolved DIA at high frequencies only, and converting this from a source term to a filter, is presented in Tolman (2008). Details of this filter will not be reproduced here.

Note that adding a filter to the NNIA in this way is expected to provide an incremental improvement to the algorithm only, because the NNIA has not been tuned explicitly with this filter, and hence may be expected to somewhat counteract the filter.

Figure 12 shows model results obtained with the NNIA including the high-frequency filter, as well as results obtained with the DIA for reference purposes. For $\epsilon_{\max} = 2.5\%$ (compare Figs 11b and 12b ) filtering has little impact on the spectral results and modestly increases the wave height. Note that this NNIA clearly reproduces results obtained with the WRT approach more closely than the DIA. For $\epsilon_{\max} = 5\%$ (compare Figs 11c and 12c ) filtering reduces spurious spectral features in the model, but does not remove the 'hole' in the spectrum.The filtering also has a positive impact on the run time of the model, as is illustrated in Table 4. The positive impact of the high-frequency filtering on the spectral shape and the model run times clearly indicates the inability of this (immature) NNIA to appropriately deal with spectral noise, and the need for a successful NNIA to explicitly deal with such noise.

Table 4: Relative run times of the wave model with various interaction approximation for case of Figs. 11 and 12. 'filt.' includes high-frequency filtering.

| | WRT | NNIA | | | DIA |
|---|---|---|---|---|---|
| | | 1.25% | 2.5% | 5.0% | |
| orig. | 1 | 0.86 | 0.77 | 0.84 | 0.012 |
| filt. | | 0.83 | 0.56 | 0.68 | |

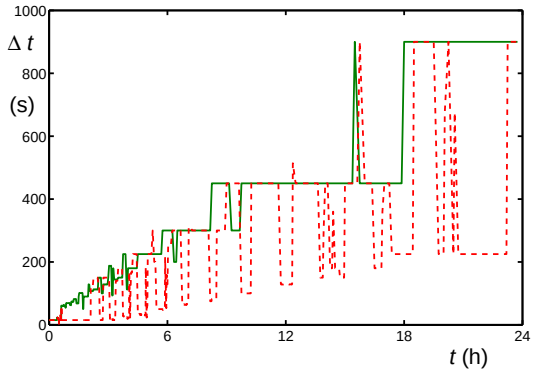


Fig. 13: Time step $\Delta t$ as a function of model integration time $t$ for model using exact WRT interaction (green solid line) or NNIA with $\epsilon_{\max} = 2.5\%$ without filtering.

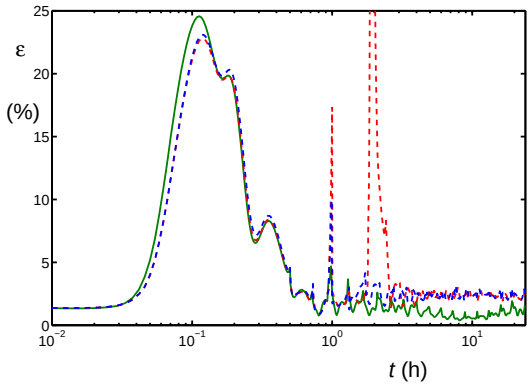


Fig. 14: Neural Network QC errors $\epsilon$ in % for WRT model integration without using NN (green line) or NNIA with $\epsilon_{\max} = 2.5\%$ (dashed lines) without filtering (red) or with filtering (blue).

The NNIA run time for a single computation is comparable to the run time of the DIA (Tolman et al., 2005). Considering this, the run times of the model using the NNIA (Table 4) are still far from the potential of the NNIA, even with the filtering applied. There are two possible explanations for this. First, QC in the NNIA may result in the NNIA to be used only sparingly, and the algorithm generally reverting to the WRT method. Second, time steps in WAVEWATCH III$^{\text{TM}}$ are computed dynamically. Noise introduced in the computations reduces time steps and hence increases model run time.

Figure 13 shows the dynamic source term integration time step $\Delta t$ as a function of the model time $t$ for a model using the WRT (solid green line) or NNIA parameterizations (dashed red line, $\epsilon_{\max} = 2.5\%$, no filtering). Using the WRT method, initial time steps are small ($\Delta t = \Delta t_{\min} = 15$s), identifying rapid changes in the spectral shapes. As time progresses, spectral changes become smaller, resulting in larger time steps. For the NNIA (dashed red line), time steps follow those of the WRT, but episodically are much smaller. This clearly indicates that noise in the NNIA systematically increases model run times.

Figure 14 presents NNIA QC errors $\epsilon$ for various model runs. The green line represent errors $\epsilon$ obtained with the WRT only (or the NNIA with $\epsilon_{\max} = 0$). The dashed red line represents errors from an NNIA with $\epsilon_{\max} = 2.5\%$ without filtering, and the blue dashed lines represents the same NNIA with filtering. To focus more on initial integration where much effort is spend due to the small time steps, a logarithmic time scale is used. Various observations can be made from this figure.

First, for initial growth ($t < 1$h) large errors $\epsilon$ occur even if the integration is not using the NNIA at all. Consequently, the NNIA will always revert to the WRT method, and the speed of the NN in the NNIA is never utilized. The large errors for initial growth indicate inaccuracies in the NN. With the NNIA design of Fig. 10 these inaccuracies can be related to either the inability of the EOFs to describe initial growth conditions, or to an underrepresentation of such conditions in the training data. Improving the NN/NNIA in this model regime will be labor intensive but fairly trivial, in particular since the NNIA objectively identifies spectra to be added to the training data set. Considering that a disproportionate part of the model integration effort is used in this computation regime, it is expected that such an improved NNIA will be significantly more economical than the NNIA used here.

Second, for larger times $t$ ($t > 1$h) errors $\epsilon$ for the WRT only model integration reduce to finite values of typically $\epsilon \approx 1 - 2\%$. This tentatively implies optimum values for $\epsilon_{\max}$, and explains run time be-

havior in Table 4. For $\epsilon_{\max} = 1.25\%$, the NN is insufficiently accurate to be used often, and hence run time improvements compared to the WRT method are minimal. For For $\epsilon_{\max} = 2.5\%$, the NN can be used often, but error growth is limited. this explains the improved run time compared to the model with $\epsilon_{\max} = 1.25\%$. For $\epsilon_{\max} = 5\%$, the NN is often engaged, but errors are allowed to grow more, apparently resulting in smaller time steps and hence no benefit in terms of model run times. Considering this, $\epsilon_{\max} = 2.5\%$ appears to be a near-optimal setting for the present NNIA.

Third, for larger times $t$ ($t > 1$h), errors of the NNIA based model (dashed lines) remain close to the prescribed maximum value ($\epsilon \approx \epsilon_{\max}$). This is indicative of cyclic behavior of the NNIA. When the NNIA is engaged, noise accumulates resulting in a decrease in time step and and increase in errors. This results in the WRT to be engaged, which smooths out the noise and reduces errors. The corresponding evolution of time steps as shown in Fig. 13 indicates that this cyclic behavior is episodic rather than more random in nature. This cyclic behavior indicates that noise accumulation in the NNIA is its main obstacle for becoming highly economical (i.e., becoming as economical as the DIA).

Fourth, the effect of filtering can be assessed by comparing the results of the NNIA without and with filtering (red and blue dashed lines, respectively). Without filtering two large error spikes occur for $t \approx 1$h and $t \approx 2$h (red line). The filtering significantly reduces the first spike, and removes the second spike (compare red and blue line). However, the filtering cannot suppress the above described cycled behavior. Hence, the present filter reduces error growth sufficiently to remove error spikes, but not sufficiently to break cyclic error growth and mitigation. As mentioned above, limited impact of the filter was expected, because the filter was not integrated in the NNIA and was not considered in the NNIA training process.

Considering the above observations, the following recommendations for future work can be made.

1) Address NNIA QC errors in initial growth by applying incremental training as naturally supported by the NNIA and by assessing possible impacts of EOF selection.

2) Assess noise sources and locations in spectral space as occur in the wave model integration.

3) Based on the above assessment, remove noise by directed training of the NNIA as far as possible.

4) Where noise accumulation cannot be removed from the NNIA, design filter techniques to reduce noise levels. It is essential, that these techniques are fully integrated in the NNIA and its training.

5) Remain focused on idealized wave growth conditions, as the behavior of interactions at different spectral scales during wave growth is a key process to be reproduced by an NNIA to be potentially successful for practical wave modeling.

6) Use NNIA QC errors directly in the development and assessment of quality of NN realizations (training).

7) Pursue the direct mapping techniques suggested by Wahle et al. (2009) to i) remove costly EOF decompositions and ii) possibly avoid EOF errors in early growth. iii) Avoid later complications expected to arise with an EOF description of multi-modal spectra.

Whereas the present NNIA is close to being able to produce acceptable interactions compared to the WRT, the present gain in model run time is clearly insufficient to justify the complication of developing and implementing this NNIA in practical wave model applications. The main issue standing between the NNIA and practical applications appears to be the development of methods to suppress or eliminate building up of noise in the spectra during model integration.

## 6 CONCLUSIONS AND OUTLOOK

The present paper documents ongoing development of the Generalized Multiple DIA (GMD) and Neural Network Interaction Approximation (NNIA) for quadruplet nonlinear wave-wave interactions in wind wave models. Development of both approximations differs from previous efforts in that progress is measured using full wave model integration rather than mapping of interactions to individual spectral. For the GMD, this results in much bigger impacts than obtained in some previous attempts. For the NNIA it is essential to prove its viability.

The GMD is nearing maturity. The algorithms are well tested and numerically optimized, and the

method is shown to be able to realistically reproduce nonlinear interactions at arbitrary depths. Objective parameter optimization techniques have been developed and are nearing maturity. Initial parameter optimization experiments show that the GMD can dramatically improve wave model behavior compared to the traditional DIA, in terms of being able to reproduce model integration results obtained with the exact WRT interaction algorithm.

The NNIA is less mature. Major progress has been made in the sense that acceptable model integrations based on an NNIA have been made. For an NNIA to be successful, it needs to have internal quality control and be able to revert to an underlying algorithm (here WRT) if the NNIA itself is found to be inaccurate. Hence, an NNIA method should be considered as a numerical accelerator of an underlying direct parameterization, rather than as a full independent interaction parameterization. The major shortcoming of the present NNIA is lack of appropriate training and the apparent accumulation of noise during model integration. The former problem can be addressed, but it will be labor intensive to do so. The latter problem will require explicit treatment of noise either within the NNIA or by filtering. The final viability of an NNIA is expected to be strongly linked to the ability to address the latter issue.

The maturity of the GMD (and other alternatives to the DIA), and the potential of the NNIA can be tested in limited ways in practical wave models, because all present physics parameterizations in such model have been tuned based on the DIA. This implies either that such physics packages should be re-tuned for better interaction approximations, are conversely, that they should be developed in a different way. A new way of developing physics packages for wave models intended to us the GMD could be:

1) Develop physics packages for idealized wave conditions and possibly limited area model applications using the exact nonlinear interactions approaches such as WRT.

2) Explicitly optimize the GMD parameters for the package as developed using exact interactions algorithms.

3) Fine tune physics parameter setting for a GMD based model for both the original test cases and full practical wave model applications.

4) If the NNIA proves successful, develop an NNIA accelerator for the nonlinear interactions in the previously developed wave model physics package and wave model application.

Note that this strategy is not dependent upon the GMD. With minor modifications it can be applied to other improved nonlinear interaction approximations. In particular, a successful NNIA can be used in conjunction with any interaction approximation.

# References


Eiben, A. E. and J. E. Smith, 2003: *Introduction to Evolutionary Computing*. Springer, 299 pp.

Hanson, J. L., B. A. Tracy, H. L. Tolman and R. D. Scott, 2009: Pacific hindcast performance of three numerical wave models. *J. Atmos. Oceanic Techn.*, **26**, 1614–1633.

Hasselmann, K., 1960: Grundgleichungen der seegangsvoraussage. *Schiffstechnik*, **1**, 191–195.

Hasselmann, K., 1962: On the non-linear transfer in a gravity wave spectrum, Part 1. General theory. *J. Fluid Mech.*, **12**, 481–500.

Hasselmann, K., 1963: On the non-linear transfer in a gravity wave spectrum, Part 2, Conservation theory, wave-particle correspondence, irreversibility. *J. Fluid Mech.*, **15**, 273–281.

Hasselmann, K., 1966: Feynman diagrams and interaction rules of wave-scattering processes. *Rev. Geophys. Space Phys.*, **4**, 1–32.

Hasselmann, K., T. P. Barnett, E. Bouws, H. Carlson, D. E. Cartwright, K. Enke, J. A. Ewing, H. Gienapp, D. E. Hasselmann, P. Kruseman, A. Meerburg, P. Mueller, D. J. Olbers, K. Richter, W. Sell and H. Walden, 1973: Measurements of wind-wave growth and swell decay during the Joint North Sea Wave Project (JONSWAP). *Ergaenzungsheft zur Deutschen Hydrographischen Zeitschrift, Reihe A(8)*, **12**, 95 pp.

Hasselmann, S. and K. Hasselmann, 1981: A symmetrical method of computing the nonlinear transfer in a gravity wave sperctrum. Hamb. Geophys. Einzelschriften, Reihe A: Wiss. Abhand. 52, 138 pp.

Hasselmann, S., K. Hasselmann, J. H. Allender and T. P. Barnett, 1985: Computations and parameterizations of the nonlinear energy transfer in a gravity-wave spectrum, Part II: parameterizations of the nonlinear energy transfer for application in wave models. *J. Phys. Oceanogr.*, **15**, 1378–1391.

Herterich, K. and K. Hasselmann, 1980: A similarity relation for the nonlinear energy transfer

in a finite-depth gravity-wave spectrum. *J. Fluid Mech.*, **97**, 215–224.

Jenkins, A. and O. M. Phillips, 2001: A simple formula for nonlinear wave-wave interactions. *Int. J. Offshore Polar Eng.*, **11**, 81–86.

Jolliffe, I., 1986: *Principle Component Analysis*. Springer Verlag.

Komen, G. J., L. Cavaleri, M. Donelan, K. Hasselmann, S. Hasselmann and P. E. A. M. Janssen, 1994: *Dynamics and modelling of ocean waves*. Cambridge University Press, 532 pp.

Krasnopolsky, V. M., D. V. Chalikov and H. L. Tolman, 2002: A neural network technique to improve computational efficiency of numerical oceanic models. *Ocean Mod.*, **4**, 363–383.

Krasnopolsky, V. M., M. S. Fox-Rabinovitz, H. L. Tolman and A. A. Belochitski, 2008: Neural network approach for robust and fast calculation of physical processes in numerical environmental models: Compound parameterizations with quality control of larger errors. *Neural Networks*, **21**, 535–543.

Krasnopolsky, V. M., H. L. Tolman and D. V. Chalikov, 2003: A combination of empirical orthogonal function and neural network approaches for parameterizing nonlinear interactions in wind wave models. in *Third Conference on Artificial Intelligence Applications to the Environmental Sciences, 83rd Annual Meeting of AMS*. AMS, Paper 3.10.

Lorenz, E. N., 1956: Empirical orthogonal functions and statistical weather prediction. Sci. Rep. 1, MIT Cambridge, Statisical Forecasting Project, 48 pp.

Resio, D. T. and W. Perrie, 1991: A numerical study of nonlinear energy fluxes due to wave-wave interactions. Part 1: Methodology and basic results. *J. Fluid Mech.*, **223**, 609–629.

SWAMP group, 1985: *Ocean wave modelling*. Plenum Press, 256 pp.

Tolman, H. L., 1992: Effects of numerics on the physics in a third-generation wind-wave model. *J. Phys. Oceanogr.*, **22**, 1095–1111.

Tolman, H. L., 2003: Optimum Discrete Interaction Approximations for wind waves. Part 1: Mapping using inverse modeling. Tech. Note 227, NOAA/NWS/NCEP/MMAB, 57 pp. + Appendices.

Tolman, H. L., 2004: Inverse modeling of Discrete Interaction Approximations for nonlinear interactions in wind waves. *Ocean Mod.*, **6**, 405–422.

Tolman, H. L., 2005: Optimum Discrete Interaction Approximations for wind waves. Part 2: Convergence of model integration. Tech. Note 247, NOAA/NWS/NCEP/MMAB, 74 pp. + Appendices.

Tolman, H. L., 2008: Optimum Discrete Interaction Approximations for wind waves. Part 3: Generalized multiple DIAs. Tech. Note 269, NOAA/NWS/NCEP/MMAB, 117 pp.

Tolman, H. L., 2009: Optimum Discrete Interaction Approximations for wind waves. Part 4: Parameter optimization. Tech. note, NOAA/NWS/NCEP/MMAB, In Preparation.

Tolman, H. L. and N. Booij, 1998: Modeling wind waves using wavenumber-direction spectra and a variable wavenumber grid. *The Global Atmosphere and Ocean System*, **6**, 295–309.

Tolman, H. L. and V. M. Krasnopolsky, 2004: Nonlinear interactions in practical wind wave models. in *$8^{th}$ international workshop on wave hindcasting and forecasting, JCOMM Tech. Rep. 29, WMO/TD-No. 1319*. Paper E1.

Tolman, H. L., V. M. Krasnopolsky and D. V. Chalikov, 2005: Neural Network approximations for nonlinear interactions in wind wave spectra: direct mapping for wind seas in deep water. *Ocean Mod.*, **8**, 253–178.

Tracy, B. and D. T. Resio, 1982: Theory and calculation of the nonlinear energy transfer between sea waves in deep water. WES Report 11, US Army Corps of Engineers.

Van Vledder, G. Ph., 2002a: Improved parameterizations of nonlinear four wave interactions for application in operational wave prediction models. Report 151a, Alkyon, The Netherlands.

Van Vledder, G. Ph., 2002b: A subroutine version of the Webb/Resio/Tracy method for the computation of nonlinear quadruplet interactions in a wind-wave spectrum. Report 151b, Alkyon, The Netherlands.

Van Vledder, G. Ph., 2006: The WRT method for the computation of non-linear four wave interactions in discrete spectral wave models. *Coastal Eng.*, **53**, 223–242.

Wahle, K., H. Gunther and H. Schiller, 2009: Neural network parameterisation of the mapping of wave spectra onto nonlinear four-wave interactions. *Ocean Mod.*, **30**, 48–55.

WAMDIG, 1988: The WAM model – a third generation ocean wave prediction model. *J. Phys. Oceanogr.*, **18**, 1775–1809.

Webb, D. J., 1978: Non-linear transfers between sea waves. *Deep-Sea Res.*, **25**, 279–298.

Zakharov, V. E. and A. N. Pushkarev, 1999: Diffusion model of interacting gravity waves on the surface of a deep fluid. *Nonlinear Proc. Geoph.*, **6**, 1–10.